Azimuthal angular dependence of recoil-ion and electron emission in 0.5-MeV p + He collisions

R. Dörner
Institut für Kernphysik, Universität Frankfurt, D6000 Frankfurt am Main, Federal Republic of Germany

J. Ullrich
Gesellschaft für Schwerionenforschung, D6100 Darmstadt, Federal Republic of Germany

R. E. Olson
Department of Physics, University of Missouri-Rolla, Missouri 65401

O. Jagutzki and H. Schmidt-Böcking
Institut für Kernphysik, Universität Frankfurt, D6000 Frankfurt am Main, Federal Republic of Germany
(Received 1 October 1992)

Measurements and n-body classical-trajectory Monte Carlo calculations are presented for the dependence of recoil-ion emission on the azimuthal angle between a projectile and a recoil ion. From the measured momenta of the projectile and the recoil ion, the dependence of the electron emission on the azimuthal angle between projectile and electron is deduced. The recoil ions are found to be emitted to the opposite direction of the scattered projectile only for scattering angles larger than 1 mrad, while for smaller scattering angles, the momentum of the emitted electron results in a broad azimuthal angular distribution of the recoil ions. For a scattering angle of 0.55 mrad, the electrons are predominantly emitted opposite to the scattered projectile, yielding a direct proof of a binary encounter between projectile and electron.

PACS number(s): 34.10.+x, 34.50.Fa

I. INTRODUCTION

Single and double ionization of helium by fast-proton impact has attracted considerable interest over the past few years. So far in literature only a few single-differential cross sections $d\sigma/d\vartheta_{\rm pro}$ [1–3] have been published, and only two experimental groups reported higher differential cross sections [4–6]. Double- and triple-differential cross sections are of particular interest because they directly reflect the importance of the electron momentum on the nuclear partners. We report here on double-differential cross sections $d^2\sigma/d\vartheta_{\rm pro}d\Phi_{\rm pro\text{-}rec}$ and $d^2\sigma/d\vartheta_{\rm pro}d\Phi_{\rm pro\text{-}e}$, i.e., the azimuthal angular distribution of recoil-ion and electron emission for fixed projectile polar scattering angle.

First single-differential cross sections $d\sigma/d\vartheta_{\rm pro}$ for single and double ionization were reported for 3- and 6-MeV proton impact by Kamber *et al.* [1] and for lower impact energies by Giese and Horsdal [2]. They show interesting structures which give hints on the mechanism of the ionization process. Kamber *et al.* found a shoulder in the single-differential cross section for single ionization at a polar scattering angle of 0.545 mrad for 3- and 6-MeV impact energy. Systematical studies showed that this structure can be found down to 0.5-MeV proton energy [3]. Several theoretical studies confirmed the explanation of this shoulder already given by Kamber *et al.* [7–10]. They showed that for projectile polar scattering angles below 0.545 mrad in the case of an ionizing collision, the dominating interaction is the proton-electron interaction. The maximum polar scattering angle for a proton scattered at an electron at rest is given by the mass ratio m_p/m_e and is 0.545 mrad. The projectile polar scattering angles larger than this critical angle must therefore be partially due to scattering by the target nucleus. For polar scattering angles below 0.545 mrad thus all nuclear impact parameters contribute to the differential cross section, while for larger angles only small impact parameters, i.e., close nuclear encounters, contribute. This leads to a sharp decrease of the differential cross section at the critical angle. This intuitive picture was experimentally confirmed by measurements of the transverse momentum, which is transferred to the recoiling He^+ ion in dependence of the projectile polar scattering angle [11,12,8]. For polar scattering angles around the critical angle of 0.545 mrad this transverse recoil-ion momentum is found to be much smaller than the corresponding projectile momentum, while for larger angles projectile and recoil-ion transverse momenta are comparable. For 3-MeV impact energy it was even possible to resolve experimentally the two processes of projectile scattering at the electron and at the target nucleus. For a fixed kinematical window, i.e., a certain azimuthal angle between scattered projectile and recoil ion and a certain polar projectile scattering angle, Gensmantel *et al.* [4] found two peaks in the transverse momentum distribution of the recoil ions, which could be associated with the projectile-electron and projectile-target nucleus interactions, respectively.

In this paper we study for 0.5-MeV p+He collisions the azimuthal angular distribution of proton, electron, and the recoiling He^+ ion emission for fixed polar

scattering angle of the projectile (see Fig. 1 for the definition of the angles). The azimuthal angular distribution of the reaction products gives direct information on the scattering process. The Q value of the collision does not influence the momentum components in the transverse direction, but only the momentum balance in beam direction (i.e., the polar angles between the particles) [13,14]. Thus each pure nuclear two-body collision (p-α collision) will lead to an azimuthal angle of 180° between projectile and recoil ion, while a binary collision between projectile and electron would lead to an azimuthal angle of 180° between projectile and electron. Therefore it should be possible to distinguish, for example, hard collisions between projectile and target electron from hard collisions between projectile and target nucleus by looking at the azimuthal angle between the particles.

The experimental data are compared to calculations made using the n-body classical-trajectory Monte Carlo (nCTMC) approach [15,10]. A microcanonical distribution is chosen for the target electrons. The binding energy is set to 0.903 a.u., equal for both electrons and a screening constant of $\frac{5}{16}$ is used. The classical equations of motion are solved, including all interactions except the electron-electron interaction. As in the experiment, the calculation gives the momenta of all particles after each collision (i.e., calculated trajectory).

II. EXPERIMENT

A recoil-ion momentum spectrometer with the target gas being cooled to a temperature of about 35 K was used in a recoil-ion projectile coincidence experiment. The experimental setup allowed for each ionizing collision the measurement of the charge state and both transverse momenta $p_{\perp \mathrm{rec}_x}$ and $p_{\perp \mathrm{rec}_y}$ of the recoil-ion and the two transverse momenta $p_{\perp \mathrm{pro}_x}$ and $p_{\perp \mathrm{pro}_y}$ of the scattered projectile (see Fig. 1 for the coordinate frame).

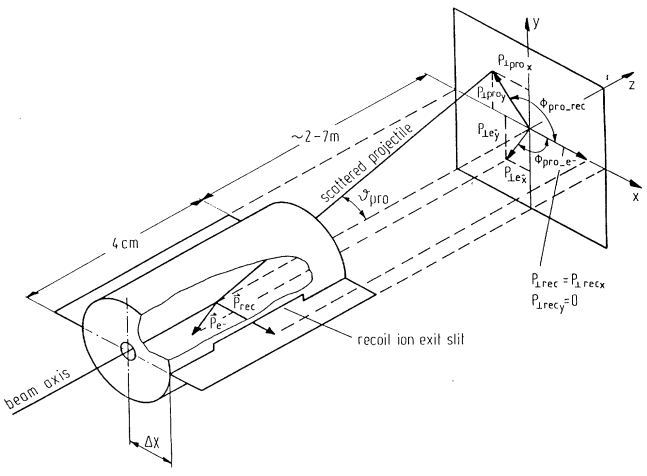

FIG. 1. Experimental geometry. For simplicity of the figure a special case where recoil ion and electron are emitted perpendicular to the beam is chosen. The recoil-ion drift path ΔX was varied in the different experiments between 2.5 and 5.5 mm. The experiment allows us to measure the projectile transverse momenta $P_{\perp \mathrm{pro}_x}, P_{\perp \mathrm{pro}_y}$ and the transverse momentum of the recoil ion $P_{\perp \mathrm{rec}}$. The coordinate frame is chosen in a way that the recoil-ion exit slit defines $P_{\perp \mathrm{rec}} = P_{\perp \mathrm{rec}_x}$ and $P_{\perp \mathrm{rec}_y} = 0$. The gas-cell cylinder is cooled to 35 K. Not shown in the figure is a magnetic field between the recoil-ion exit slit and the position-sensitive channel-plate detector for the recoil-ion charge-state separation.

The experiment was performed at the 2.5-MV van de Graaf accelerator of the Institut für Kernphysik in Frankfurt. The proton beam was collimated to a divergence of less than 0.1 mrad. After passing through the target gas cell the protons were detected 2.7 m downstream by a two-dimensional position-sensitive channel-plate detector. For some part of the experiment the beam of unscattered protons was stopped on a cross of wires with a 0.5 mm diameter in front of the detector. Using a wedge and strip anode, a position resolution of ≤ 0.2 mm full width at half maximum was achieved. During the experiment a projectile rate of 2000–10 000 Hz was detected. The recoil-ion transverse momentum was measured using a time-of-flight technique. The recoil ions are produced in a cylindrical gas cell of 10 mm diameter and 40 mm length. They drift from the beam axis to the cylinder wall and can only exit the gas cell through a slit of 1 mm × 20 mm parallel to the beam axis. The gas cell is kept on an electric potential of +500 V. Outside the drift region the ions are accelerated in a homogeneous electrostatic field down to ground potential. After passing an einzellens they are charge-state analyzed in a magnetic field and detected by a two-dimensional position-sensitive channel-plate detector. To avoid leakage of the acceleration field inside the drift region, the exit slit is covered with a copper grid (mesh width 0.12 mm × 0.12 mm). The potential drops to a value of 5 mV within 0.4 mm. For the calculation of the residual field inside the spectrometer see Fig. 5 in [16]. For this experiment it is essential that all, i.e., slow and fast, recoil ions are detected with the same geometrical solid angle, which is given by the beam position and the exit slit, and that slow recoil ions are not sucked out of the gas cell by the acceleration field. Therefore systematical experimental tests were made to control this. For example, the acceleration field was changed by about a factor of 5 without significant change in the recoil-ion count rate and the deduced momentum distribution.

All recoil ions with polar angles between 20° and 160° are detected with constant efficiency. To ensure a Faraday cage free of electric fields even on the mV level, the spectrometer gas cell is gold coated and was carefully cleaned in a supersonic bath before each experiment.

To achieve a sufficient recoil-ion momentum resolution to resolve the azimuthal angular distributions of the recoil ions, it is indispensable to cool the target gas. A scattering angle of 0.5 mrad for 0.5 MeV $p \rightarrow$He corresponds to an energy of the recoil ion of 31 meV if a two-body collision is assumed. The transverse component of the thermal motion at room temperature results in a mean energy of 25 meV. By mounting the spectrometer gas cell on the cold finger of a cryopump and precooling the target gas before entering the gas cell, a gas temperature of 35 K was achieved. By repeating the experiment several times with different flight paths (2.5, 3.5, and 5

mm) and with different spectrometer materials, we estimate the effect of internal electric fields in the gas cell to be $\leq \pm 5$ meV. The gas pressure in the target cell was about 0.1 Pa. This is low enough to have single-collision conditions for the projectiles and to ensure that the recoil ions do not undergo charge exchange on their way from the beam axis to the recoil-ion exit slit. The latter was checked in two ways. First the ratio He^{2+} to He^{+} was found to be pressure independent in the pressure regime used. If a recoil ion has a collision with another target atom in the drift region, the ion loses energy and changes its direction of flight and therefore has a longer flight time. Only for pressures more than ten times higher than our normal pressure did a tail of such slow recoil-ions appear in the time-of-flight spectrum. For a more detailed discussion of the spectrometer see [16].

For single ionization the momentum balance in the plane perpendicular to the beam axis is experimentally completely determined. The transverse momentum components of the ejected electron $p_{\perp e_x}$ nd $p_{\perp e_y}$, although it is not detected in the experiment, can be derived from the measured momentum components of the heavy particles using momentum conservation:

$$p_{\perp e_x} = -(p_{\perp \mathrm{rec}_x} + p_{\perp \mathrm{pro}_x}) , \quad (1)$$

$$p_{\perp e_y} = -(p_{\perp \mathrm{rec}_y} + p_{\perp \mathrm{pro}_y}) . \quad (2)$$

Although there is no principle restriction for this indirect method to obtain electron spectra, it is limited in practice to cases where $p_{\perp \mathrm{rec}_{x,y}}$ and $p_{\perp \mathrm{pro}_{x,y}}$ are not too large compared to $p_{\perp e_{x,y}}$.

III. RESULTS AND DISCUSSION

In order to allow for a qualitative comparison with theory it is imperative to correctly calculate the influence of the experimental resolution on the results. Since the CTMC calculations give the final momenta of all emitted particles after the collision, they turned out to be well suited to study the effects of the residual thermal motion of the target atom before the collision, the beam divergence, the projectile detector resolution, and the azimuthal recoil-ion acceptance. The experimental situation was simulated by adding randomly chosen momenta to the calculated recoil-ion and projectile momenta after the collision. The distribution for the momenta added to the recoil ion in all three dimensions reflects the Maxwell distribution, and the distribution of the additional projectile momenta is assumed to be Gaussian in both dimensions with a width given by the experimental resolution. In addition to this the recoil-ion azimuthal angle was smeared out by $\pm 6°$ as given by the geometry of the recoil-ion exit slit.

As discussed in the Introduction, for 0.5-MeV impact energy the single-differential cross section in dependence of the projectile polar scattering angle shows no distinct structure [Fig. 2(a)]. Since the cross section drops by more than three orders of magnitude between 0 and 2 mrad, the experiment was performed in two steps. In a first experiment the beam was cut down to an intensity of about a few thousand particles per second, and the full beam was detected by the position-sensitive channel-plate detector. Due to the small solid angle and the low target gas pressure, the coincidence countrate is below 1 Hz in this case. The differential data are normalized to a total cross section of $(3.70 \pm 0.15) \times 10^{-17}$ cm^2 as given in Ref. [17]. In a second experiment the undeflected beam was dumped on a cross of wires with a 0.5 mm diameter. The data points below 0.6 mrad are measured without the beam dump. The data for larger polar scattering angles are measured with the beam dump and connected to the first experiment at 0.55 mrad. From the systematical arrow of the total cross section [17] and from our tests of the independence of the spectrometer solid angle with $p_{\perp \mathrm{rec}}$ as discussed in Sec. II, we estimate the systematical

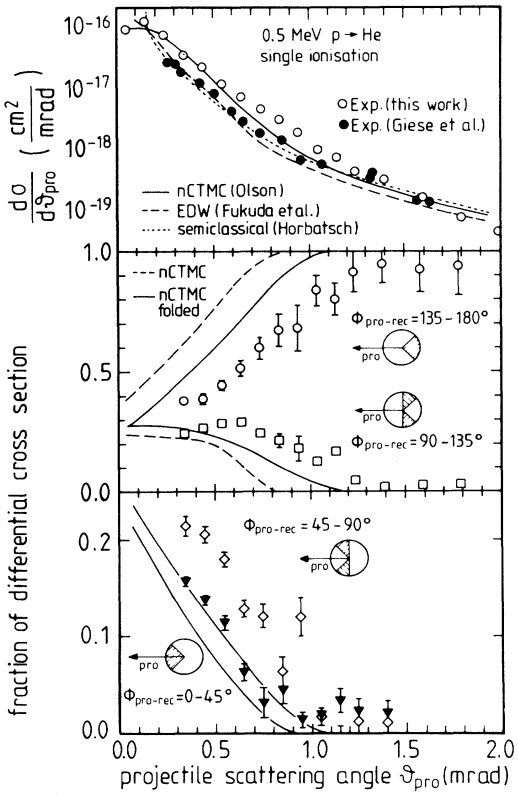

FIG. 2. (a) Single-differential cross section for 0.5-MeV $p + \mathrm{He} \rightarrow p + \mathrm{He}^{+}$. Open circles, this experiment; points, experimental data by Giese and Horsdal [2]; full line, *n*CTMC calculation [10]; dashed line, eikonal distorted-wave calculation [8]; dotted line, quantum statistical model [18]. (b) and (c) Fraction of the differential cross section into two different azimuthal angular regions $\Phi_{\text{pro-rec}}$ between projectile and recoil ion. Open circles, $135° < \Phi_{\text{pro-rec}} < 225°$; open squares, $90° < \Phi_{\text{pro-rec}} < 135°$ or $225° < \Phi_{\text{pro-rec}} < 270°$; open diamonds, $45° < \Phi_{\text{pro-rec}} < 90°$ or $270° < \Phi_{\text{pro-rec}} < 315°$; full triangles, $0° < \Phi_{\text{pro-rec}} < 45°$ or $315° < \Phi_{\text{pro-rec}} < 360°$. The azimuthal angular regions are indicated by the shaded area in the circle. Dashed line, *n*CTMC calculation; full line, *n*CTMC calculation folded with the experimental resolution of ± 0.07 mrad for the projectile detection and thermal distribution of 35 K for the target atom initial motion and an azimuthal acceptance angle for the recoil ions of $\pm 8°$.

error of our data points below 0.55 mrad to be less than ±30%. For the data points above 0.55 mrad an additional error of ±15% arises due to the connection of the two experiments.

The data show a deviation of up to a factor of 2 from the data of Giese and Horsdal [2]. The reason for this discrepancy is not obvious to us. The full line shows the *n*CTMC results [10], the dashed line shows an eikonal distorted-wave calculation by Fukuda *et al.* [8], and the dotted line shows the results of the quantum-statistical model from Horbatsch [18]. Within the experimental uncertainty all three theoretical models agree well with the experimental results. The maximum in the experimental cross section at 0.15 mrad is very likely to be due to the spatial resolution of the projectile detector and the beam divergence. The finite experiment resolution for the projectile transverse momentum measurement of $\pm 0.07 \times 10^{-3} p_{\perp \mathrm{pro}_{x,y}} / p_0$ (p_0 is the projectile longitudinal momentum) can produce such a maximum, when the momenta are transformed from Cartesian to polar coordinates.

In Figs. 2(b) and 2(c) it is illustrated how the different regions of azimuthal angular scattering between projectile and recoil ion contribute to the differential cross section with varying polar projectile scattering angle. For this purpose the azimuthal angles, i.e., the plane perpendicular to the beam axis, is divided into eight sectors of 45°. Since the beam was not polarized, the experiment should be symmetric to the $X-Z$ plane (see Fig. 1). Therefore the corresponding sectors are added [see shaded areas in Figs. 2(b) and 2(c)]. $\Phi_{\text{pro-rec}}=0°$ denotes the situation where recoil ion and projectile are emitted in the same direction. It can be seen from Fig. 2(b) that the polar scattering angle regime above 1.2 mrad can clearly be associated with hard collisions between projectile and target nuclei. For nearly all ionizing collisions leading to scattering angles above 1.2 mrad the recoil ions are emitted to azimuthal angles between 135° and 225° with respect to the scattered projectile. This is in good agreement with experimental results and theoretical predictions obtained for the mean recoil-ion energy for these scattering angles [11,12,8]. For polar scattering angles ϑ larger than 1.2 mrad the mean recoil-ion transverse energy $\langle E_{\perp \mathrm{rec}} \rangle$ is very close to

$$E_{\perp \mathrm{rec}} = E_{\mathrm{pro}} \frac{m_{\mathrm{pro}}}{m_{\mathrm{rec}}} \tan^2 \vartheta_{\mathrm{pro}} , \tag{3}$$

which is expected from momentum conservation for a two-body momentum exchange between projectile and target nuclei.

For polar scattering angles below 1.2 mrad the recoil-ion emission tends to get more and more isotropic in the plane perpendicular to the beam axis. This strongly supports the intuitive picture of the importance of the projectile electron scattering for small scattering angles. Since for small scattering angles the momentum exchange between projectile and the ejected electron is for most ionizing collisions much larger than the momentum exchange between the scattered projectile and the target nucleus, the two heavy particles are no longer necessarily emitted back to back. In this scattering angle regime the corresponding recoil-ion energy is much lower than expected from Eq. (3).

The full line in Fig. 2(b) shows the result of the *n*CTMC calculation. The classical calculations reproduce the transition from nearly isotropic recoil-ion emission for small scattering angles to back-to-back emission for large scattering angles as found in the experiment. Since the interaction between projectile and both electrons, projectile and target nucleus, and recoiling ion and emitted electron are fully incorporated in these calculations, the *n*CTMC is able to predict the transition from mainly projectile electron scattering at small polar scattering angles to the region of hard nuclear encounters at large polar scattering angles.

To see how the experimental resolution in the projectile momentum and the recoil-ion momentum (thermal motion) influences the results, the dashed line shows the *n*CTMC results folded with the projectile momentum resolution of ±0.6 a.u. (which corresponds to ±0.07 mrad) and a target temperature of 35 K. Although the target gas is cooled, there is still a considerable influence of the thermal motion on the measured azimuthal angular distributions. But even if the effect of the resolution is taken into account, some discrepancy between experiment and *n*CTMC prediction remains. It seems as if the classical calculation underestimates the influence of the ejected electron on the trajectories of the heavy particles. Up to now there are no results of a full quantum-mechanical calculation available for the azimuthal angular dependences discussed. However, quantum-mechanical calculations were done for the dependence of the mean electron energy of the projectile polar scattering angle [7,8]. Both quantum-mechanical calculations predict up to a factor of 2 higher mean electron energies for polar scattering angles above 0.4 mrad than found in the *n*CTMC model. For 0.55 mrad the mean electron energy reaches its maximum due to the hard binary-encounter processes, which are accumulated at this angle. The *n*CTMC result for the mean electron energy at this angle is 200 eV, the prediction of the eikonal distorted-wave approximation [8] is about 300 eV. For scattering angles above 1 mrad the quantum-mechanical calculations give a mean energy of around 140 eV in contrast to only about 70 eV in the *n*CTMC approach. The results of the azimuthal angular dependence of the recoil-ion emission presented here thus support the prediction of higher electron momenta of the quantum-mechanical calculations in contradiction to the *n*CTMC.

Figure 3 shows the azimuthal angular dependence of the recoil-ion emission for different polar scattering angles in a polar plot. To eliminate errors due to the partial shading of the projectile detector by the wire, which was used to block the unscattered beam, recoil-ion time-of-flight spectra were created in the data analysis for each polar and azimuthal angular window. The data in Fig. 3 show the ratio of true to random coincidences in these time-of-flight spectra. For each polar scattering angle the integral over all azimuthal angles is normalized to the experimental differential cross section [Fig. 2(a)]. In this way the data of Fig. 3 are free from any shading effects on the projectile detector.

For 1.8-mrad polar scattering angle, corresponding to a transverse momentum $p_{\perp\text{pro}}$ of 15.5 a.u. and an impact parameter of 3200 fm calculated with an unscreened Coulomb potential, the recoil ions are ejected sharply opposite to the projectile. The momentum of the ejected electron is small compared to the momenta of the heavy particles and has only a minor influence on the projectile and recoil-ion trajectories. Going to smaller scattering angles, the azimuthal angular distribution gets broader. For polar scattering angles below 0.7 mrad we found with decreasing projectile scattering angle an increasing number of recoil ions which are emitted to the same hemisphere as the projectile. A similar phenomenon of "negative scattering angles" has been predicted for the system $U^{32+}+Ne$ [19]. For the highly charged ion impact, however, this predicted effect is due to a strong polarization of the target electron cloud before the ionization, while for the $p\rightarrow$He case the negative scattering angles are due to a hard collision between projectile and the ejected electron.

It is obvious from the broad azimuthal distribution of the recoil ions that neither the scattering plane, i.e., the plane defined by the beam axis and the internuclear vector before the collision, nor the impact parameter to the target nucleus can be obtained by detecting the scattered projectile for these small scattering angles. The projectile scattering in this case is more sensitive to the impact parameter with respect to the electron than to the nuclear impact parameter. The *n*CTMC calculations indicate that the nuclear impact parameter is more closely related to the recoil-ion momentum than to the projectile polar scattering angle [13].

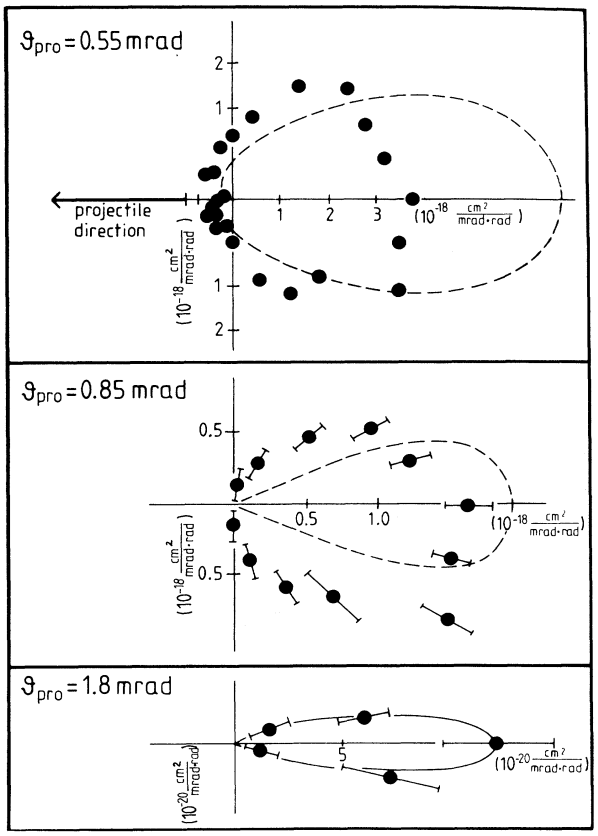

FIG. 3. Polar representation of the azimuthal angular dependence ($\Phi_{\text{pro-rec}}$; see Fig. 1) of recoil-ion emission for three different polar projectile scattering angles (ϑ_{pro}). Note that the distance of the data points from the origin is proportional to the double-differential cross sections $d^2\sigma/(d\vartheta_{\text{pro}}d\Phi_{\text{pro-rec}})$ and not the modulus of the recoil-ion momentum. Dashed line, *n*CTMC calculation, folded with the experimental resolution (same as in Fig. 2); full line, line to guide the eye.

The theoretically predicted evolution of the recoil-ion azimuthal angular distribution to nearly isotropic emission for $\vartheta_{\text{pro}}\rightarrow 0$ is shown in Fig. 4. For very small ϑ_{pro} no comparison to the experiment is possible due to the limitation of the experimental resolution even after cooling of the target gas. For the larger scattering angles the comparison with the experimental data is shown in Fig. 3. The calculated effect of the experimental accuracy of recoil ion and projectile momentum measurement is shown by the dashed line. Note that the folding of the theoretical results with the experimental resolution in Figs. 4 and 5 has two effects: (i) the thermal motion broadens the angular distribution and (ii) the limited projectile momentum resolution broadens the distribution too and increases the cross section in this angular regime because the single differential cross section is very steep here.

From the importance of the projectile electron momentum exchange we expect that the electron emission shows a strong anisotropy in the azimuthal angle with respect to the projectile ($\Phi_{\text{pro-}e}$) at least for projectile polar scattering angles between 0.1 and 1.2 mrad. Since a coincidence experiment is necessary, there are, to our knowledge, for fast ion-atom collisions no results of direct measurements of the azimuthal angular dependence of ionization electrons published in literature. As described in Sec. II, it is possible to obtain for single ionization the transverse momentum components of the emitted electrons from the measured transverse momenta of the projectile and recoil ion. Figure 5 shows the azimuthal emission pattern of the electrons for a fixed polar projectile scattering angle of 0.55 mrad. These double-differential cross sections $d^2\sigma/d\vartheta_{\text{pro}}d\Phi_{\text{pro-}e}$ have been obtained the following way. For each ionizing collision first the momentum components $p_{\perp e_{x,y}}$ and from this the angle $\Phi_{\text{pro-}e}$ for this event have been calculated. Then all recorded scattering events with $0.5\text{ mrad}<\vartheta_{\text{pro}}<0.6$ mrad have been sorted with respect to its calculated $\Phi_{\text{pro-}e}$. Due to this procedure the double-differential cross section is normalized to the single differential cross section at $\vartheta_{\text{pro}}=0.55$ mrad from Fig. 2(a).

As expected the experimental data show a strong anisotropy. For a polar projectile scattering angle of 0.55 mrad the electrons are emitted predominantly opposite to the scattered projectile. This strong correlation between projectile and target electron once again highlights that it is impossible to relate these small scattering angles to a nuclear impact parameter.

The two data point closest to $\Phi_{\text{pro-}e}=180°$ fall off the line one would expect from the rest of the data. In most of the ionizing collisions which contribute to the double-

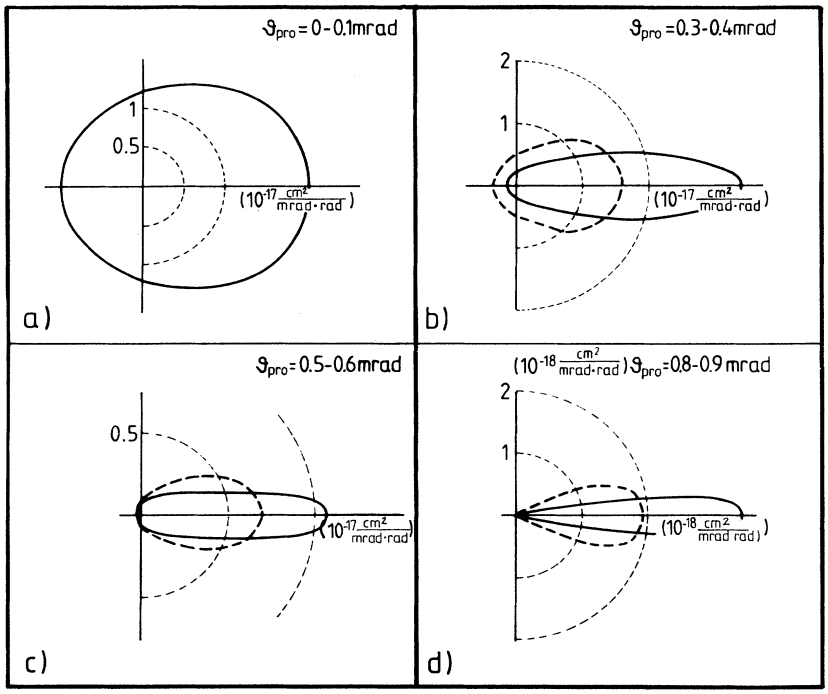

FIG. 4. Polar presentation of $d^2\sigma/(d\vartheta_{pro}d\Phi_{pro\text{-}rec})$ (same as in Fig. 3). Full line, *n*CTMC; dashed line, *n*CTMC folded with the experimental resolution (same as in Fig. 2).

differential cross section in Fig. 5 around $\Phi_{pro\text{-}e}=180°$, $p_{\perp rec}$ is very small (for $p_{\perp rec}=0$ it follows $\Phi_{pro\text{-}e}=180°$ from the conservation of momentum). Thermal motion, as well as any attractive potential in direction of the recoil-ion exit slit, leads to an increase of the measured $p_{\perp rec}$, reduces the number of events with very small $p_{\perp rec}$, i.e., with $\Phi_{pro\text{-}e}$ close to 180°, and increases the number of events with larger $p_{\perp rec}$. This effect could be a possible reason why the two data points around $\Phi_{pro\text{-}e}=180°$ show an unexpected low cross section. The *n*CTMC calculation reproduces this strong anisotropy of the electron emission. From Figs. 3 and 5 it can be seen that for the ionizing collisions which lead to projectile scattering angles around 0.55 mrad the electron and the recoil ion are both emitted dominantly to the same hemisphere, opposite to the scattered projectile. The calculations predict, however, that for $\vartheta_{pro}\rightarrow 0$ this picture changes. For very small scattering angles the recoil ion and the electron are expected to be emitted more likely back to back, balancing each others momentum (see the discussion in [11]).

IV. CONCLUSION

Absolute double-differential cross sections in dependence of projectile polar and azimuthal angle for recoil-ion emission for the single ionization of helium by 0.5-MeV photon impact have been measured using a projectile–recoil-ion coincidence technique with a cooled target. From the measured recoil-ion and projectile transverse momenta also the azimuthal angular dependence of the electron emission for a fixed projectile polar scattering angle could be deduced. The azimuthal angu-

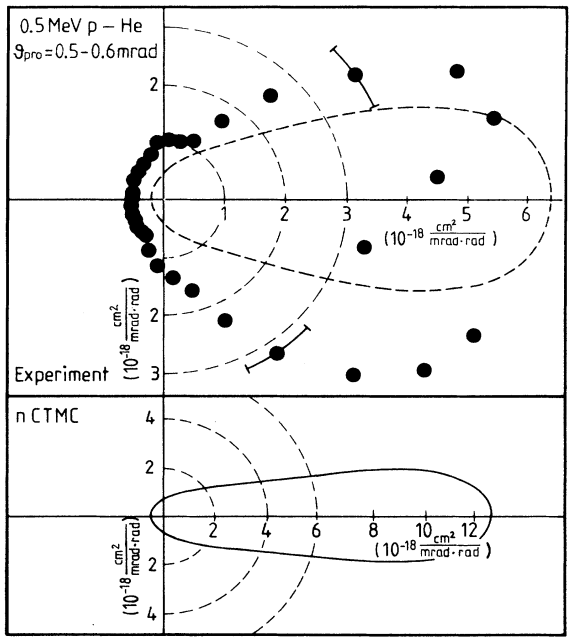

FIG. 5. Azimuthal angular dependence of electron emission relative to the projectile ($\Phi_{pro\text{-}e}$) for fixed polar projectile scattering angle 0.5 mrad $<\vartheta_{pro}<0.6$ mrad. Upper figure: circles, experiment; dashed line, *n*CTMC calculation folded with the experimental resolution (see Fig. 2) and multiplied by 0.5. Lower figure: *n*CTMC calculation.

lar dependence of the recoil ions depends strongly on the projectile polar scattering angle. The data show that for all scattering angles below 1.2 mrad, the recoil-ion emission is not dominated by projectile–target-nucleus momentum exchange. With decreasing projectile transverse momentum the azimuthal recoil distribution gets broader. A significant part of ionization events with negative scattering angles, i.e., events where projectile and target are emitted to the same direction, is observed. Therefore the information about the scattering plane and the nuclear impact parameter cannot be extracted from the projectile scattering for the dominating fraction of the total cross section. As a consequence calculations done in the impact-parameter approximation cannot be compared directly with differential experimental data, but have to be transformed to the projectile scattering picture explicitly [8,7,18].

An azimuthal angular dependence of the electron emissions for a fast heavy-ion–atom collision has been obtained experimentally. Without directly measuring the emitted electron, its momentum vector in the plane perpendicular to the beam direction could be extracted from the measured projectile and recoil ion momenta. This method is of great importance for future experimental work on multiple ionization, since it allows us to determine the sum momentum of all electrons emitted in a collision (for application see [20,21,13]). It opens a chance to gain information on the angular correlation between the electrons in a multiply ionizing collision without a multiple coincidence, which detects all electrons of the collision. For the helium single ionization, the electrons for a polar projectile scattering angle of around 0.55 mrad are found to be emitted dominantly opposite to the scattered projectile, as expected from a binary projectile-electron collision.

ACKNOWLEDGMENTS

The work was supported by the Deutsche Forschungsgemeinschaft, the Bundesministerium für Forschung und Technologie, the Office of Fusion Energy of the U.S. Department of Energy, and the National Science Foundation under Grant No. INT 9112815.

[1] E. Y. Kamber, C. L. Cocke, S. Cheng, and S. L. Varghese, Phys. Rev. Lett. **60**, 2026 (1988).
[2] J. P. Giese and E. Horsdal, Phys. Rev. Lett. **60**, 2018 (1988).
[3] F. G. Kristensen and E. Horsdal-Pedersen, J. Phys. B **23**, 4129 (1990).
[4] A. Gensmantel, J. Ullrich, R. Dörner, R. E. Olson, K. Ullmann, E. Forberich, S. Lencinas, and H. Schmidt-Böcking, Phys. Rev. A **45**, 4572 (1992).
[5] B. Skogvall and G. Schiewietz, Phys. Rev. Lett. **65**, 3265 (1990).
[6] G. Schiwietz, J. Phys. A **37**, 370 (1988).
[7] A. Salin, J. Phys. B **22**, 3901 (1989).
[8] H. Fukuda, I. Shimamura, L. Vegh, and T. Watanabe, Phys. Rev. A **44**, 1565 (1991).
[9] X. Fang and J. F. Reading, Nucl. Instrum. Methods B **53**, 453 (1991).
[10] R. E. Olson, J. Ullrich, R. Dörner, and H. Schmidt-Böcking, Phys. Rev. A **40**, 2843 (1989).
[11] R. Dörner, J. Ullrich, H. Schmidt-Böcking, and R. E. Olson, Phys. Rev. Lett. **63**, 147 (1989).
[12] R. Dörner, J. Ullrich, O. Jagutzki, S. Lencinas, H. Schmidt-Böcking, and R. E. Olson, Z. Phys. D **21**, 57 (1991).
[13] R. Dörner, J. Ullrich, O. Jagutzki, S. Lencinas, A. Gensmantel, and H. Schmidt-Böcking, in *Invited Papers of the Seventeenth International Conference on the Physics of Electronic and Atomic Collisions,* edited by W. R. MacGillivray, I. E. McCarthy, and M. C. Standage (Hilger, Bristol, 1991), p. 351.
[14] R. Ali, V. Frohne, C. L. Cocke, M. Stöckli, S. Cheng, and M. L. A. Raphaelian, Phys. Rev. Lett. **69**, 2491 (1992).
[15] R. E. Olson, J. Ullrich, and H. Schmidt-Böcking, Phys. Rev. A **39**, 5572 (1989).
[16] J. Ullrich, R. Dörner, S. Lencinas, O. Jagutzki, H. Schmidt-Böcking, and U. Buck, Nucl. Instrum. Methods B **61**, 415 (1991).
[17] M. B. Shah and H. B. Gilbody, J. Phys. B **18**, 899 (1985).
[18] M. Horbatsch, J. Phys. B **22**, L639 (1989).
[19] J. Ullrich, R. E. Olson, R. Dörner, V. Dangendorf, S. Kelbch, H. Berg, and H. Schmidt-Böcking, J. Phys. B **22**, 627 (1989).
[20] E. Forberich, R. Dörner, J. Ullrich, R. E. Olson, K. Ullman, and A. Gensmantel, J. Phys. B **24**, 3613 (1991).
[21] A. D. Gonzales, S. Haagmann, T. B. Quinteros, B. Krässig, R. Koch, A. Skutlartz, and H. Schmidt-Böcking, J. Phys. B **23**, L303 (1990).